ACTA IMEKO
ISSN: 2221-870X
March 2026, Volume 15, Number 1, 1 - 7

Optimization of the estimation and compensation algorithm for dynamic digital image correlation measurements

Giovanni Sala[1], Simone Paganoni[1], Emanuele Zappa[1]

[1] *Department of Mechanical Engineering, Politecnico di Milano, Milan, Italy*

ABSTRACT
In the last two decades, the interest in digital image correlation (DIC) has grown steadily in various industrial and scientific fields, thanks to its contactless nature, capability to provide full field measurements, and ease of implementation. The possibility to carry out measurements in the presence of significant relative motion between the camera and the target has been thoroughly investigated. In dynamic conditions, the main additional source of uncertainty is represented by the motion blur effect, which is experienced whenever the relative displacement between the camera and the target during the exposure time is not negligible. Motion blur is a source of uncertainty, since it decreases the contrast in the image and the definition of the speckles in the acquired pattern. In this work, a complete procedure for motion blur estimation and compensation is considered. It was found that the uncertainty in the estimation of the blur intensity and orientation plays a crucial role in motion blur compensation. In this work, we propose a technique for the optimization of the blur estimation and compensation phases based on fitting the motion optical transfer function to a motion model. Compensation with a Wiener filter is then performed, studying different approaches to image noise estimation. Results show that the optimized procedure has a positive effect on DIC performances, being able to reduce the effect of motion blur on uncertainty, in particular for motion blur levels larger than about 1–2 px. The entire work has been validated by considering the procedure performances on DIC analysis performed on different kinds of speckle image with various amounts of motion blur applied.

Section: RESEARCH PAPER

Keywords: digital image correlation; dynamic measure; measurement; motion blur; motion estimation; motion compensation

Citation: G. Sala, S. Paganoni, E. Zappa, Optimization of estimation and compensation algorithm for dynamic digital image correlation measurements, Acta IMEKO, vol. 15 (2026) no. 1, pp. 1-7. DOI: 10.21014/actaimeko.v15i1.1930

Section Editor: Francesco Lamonaca, University of Calabria, Italy

Received September 6, 2024; **In final form** December 14, 2025; **Published** March 2026

Corresponding author: Simone Paganoni, e-mail: simone.paganoni@polimi.it

1. INTRODUCTION

Digital image correlation (DIC) is a non-contact, image-based optical method for full-field shape, displacement, and deformation measurements [1].

To carry out a DIC analysis, the surface of the target must show a proper speckle to guarantee a unique correspondence between the different subsets in the two images [2]. Dong et al. [3] pointed out a list of prerequisites that the speckle pattern should comply with, to avoid the correspondence problem.

In some applications, the motion of the target during the camera shutter time cannot be considered negligible. In recent years, the interest in the dynamic applications of DIC has also increased [4]. For instance, tasks related to modal analysis are considered in [5], [6], [7], while the possibility to perform structural assessment using cameras mounted on drones is studied in [8], [9], [10]. Rotating blades measurements using DIC are performed in [11], [12]. When dealing with dynamic measurements, in addition to the usual sources of uncertainty that are present in the static field (e.g. noise, out-of-plane displacements of the target, optical aberrations of the acquisition camera), there are supplementary sources of error which are strictly attributable to the fact that the target is moving. Lavatelli et al. [13] proposed a theoretical framework aimed at describing the uncertainty introduced by the motion of the target, starting from an analytical description of the motion blur phenomenon. According to that work, the error due to motion introduced in the measurement of the position of a unidirectionally vibrating target with law $x(t) = A_0 \sin(\omega t)$ is composed of two components: the static and the dynamic one.

In particular, the dynamic component takes account of the fact that the exposure time is not actually infinitesimal, giving rise to the motion blur effect. From the visual point of view, the outcome of the convolution operation will be the image blurred with trails in the direction of the motion (Figure 1).

In a further work [14], the authors investigated the dependence of the uncertainty on the sum of square of the

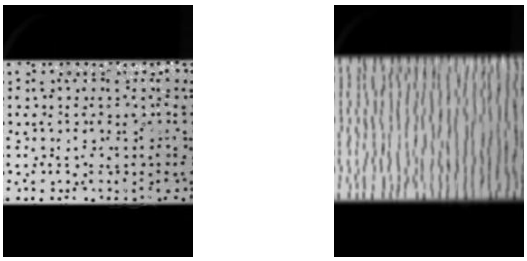

Figure 1. Example of motion blur on a vibrating target.

subset intensity gradient (SSSIG), which can be described as an index of the image contrast. In case of motion blur, the SSSIG of the image is demonstrated to be reduced, leading to an increase of the uncertainty.

Even if based on two different frameworks, the above results point out how detrimental the motion of the target is for DIC measurements and, consequently, the potential gain that can be obtained by correcting the motion blur effect, thus justifying the effort put into it.

To correct the motion blur, the first step is to estimate it, which means to estimate the amount of space covered by the target during the exposure time. In literature, two main approaches to this can be found: blind and referenced methods. The former attempts to estimate the blur directly from the blurred image [15], while the latter is based on the comparison with an image of the target in still position. In DIC applications, the referenced method appears more suitable since, on one hand, a non-blurred reference image is usually available (used as reference in the DIC analysis), and, on the other hand, image artifacts usually introduced by blind methods can be avoided.

In the framework of referenced estimation, the aim is the experimental identification of the convolution window that links reference and blurred images. This can be done in different ways, usually developed in the frequency domain. In [16], a method based on the calculation of cepstrum is proposed, while a more straightforward approach is the calculation of the ratio between the Fourier transforms (FTs) of the reference image and the blurred one. Regardless of how the convolution window is experimentally evaluated, both techniques involve the fitting of the convolution function to a sinc function (section 2.1) to retrieve the motion blur parameters. In this work, the estimation trough the FTs has been employed, and the fitting procedure will be explained in section 3.1.

Once the blur parameters have been found, it is possible to remove the blur effect. A possible approach is the inverse application of the estimated convolutional windows, possibly in Fourier domain. An example of this approach is presented in [16], with the compensation carried out in cepstrum domain. While being quite simple, this technique has the main drawback of not being able to reject the noise in the image, therefore it gives worse results as the noise level in the image increases. This problem can be reduced by performing the deblurring using a Wiener filter [17].

2. MOTION BLUR MODELLING AND SIMULATION

2.1. Analytical model

The motion blur effect is experienced every time there is a relative motion between the target and the camera during the exposure time, that is, the time interval in which the shutter of the camera is open. As anticipated, in a motion-blurred image, the objects in the scene will show a "wake" along the direction of the motion, of length equal to the space covered during the shutter time, W. To analytically model the effect, the image formation process can be taken into account [18]. When the speed of the target can be assumed constant during the exposure time, the motion blur can be modelled as a 2D convolution between the original still image and a 2D rectangular window, of length equal to $\mathrm{W} = \mathrm{v} \cdot t_{\mathrm{sh}}$, where v is the target speed in $\mathrm{px/s}$ and t_{sh} is the shutter time in seconds.

In Fourier domain, this convolution corresponds to the product of the spectrum of the still image and an optical transfer function (OTF). OTF is the Fourier transform of the 2D rectangular window. The expression of motion OTF is [19]:

$$\mathcal{H}(k,l) = \mathrm{sinc}[W \cdot (\sin(\phi) \cdot k + \cos(\phi) \cdot l)]\,, \tag{1}$$

where k and l are the spatial frequencies (in $\mathrm{px^{-1}}$) along the horizontal and vertical directions, respectively, ϕ is the direction of the motion, that is, the counterclockwise angle that motion wake forms with respect to horizontal direction. Figure 2 shows an example of the theoretical amplitude of motion OTF.

The sinc function has useful properties that can be used to obtain motion parameters W and ϕ. It can be shown that the width of the main lobe of the sinc function is equal to $\frac{2}{W}$. Another useful property comes from the observation that its maximum is 1, and it is reached when the argument is null. Imposing this condition, it is possible to show that the locus of points for which the sinc function reaches its maximum is a straight line, the equation of which can be expressed as:

$$k = -\frac{1}{\tan(\phi)} \cdot l\,. \tag{2}$$

Defining ψ as the inclination of this line, that is, the inclination with respect to horizontal of the main lobe stripe, the previous equation shows how ψ is related to the motion direction ϕ by the following relation:

$$\Psi = \phi + \frac{\pi}{2}. \tag{3}$$

In real cases, motion blur is usually associated with an amount of rigid motion (that is, the displacement search for instance with DIC). To account for this rigid displacement, the 2D rectangular window, still of length W, is not centered in zeros, but it is shifted in space domain by a quantity equal to the rigid motion. In Fourier domain, this shift corresponds to a linear trend added to the phase of the OTF along the direction of the motion [20]. This trend does not actually affect the amplitude of the OTF.

2.2. Simulation techniques

To numerically apply blur on an image, several techniques are available. Considering what was said in the previous section, a straightforward technique is to multiply the spectrum of the reference image by the sinc function corresponding to the amount of motion blur W that it is intended to blur the image with. In order to come back to the space domain, it is sufficient to evaluate the discrete inverse Fourier transform of the product thus obtained, which will be the blurred image. However, this approach is restricted to the case of constant and uniform speed during exposure time. A more general approach is the so-called averaging technique [14], which is based on the average of multiple images shifted in space by sub-pixel amounts, to reproduce real target motion during exposure time. The

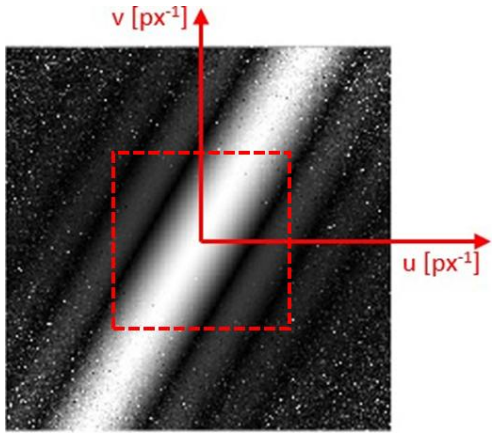

Figure 2. Example of the amplitude of the experimental motion OTF for $W = 8\,px$ and $\phi = 60°$. The dotted rectangle shows an example of cutting window used to select lower frequency region for sinc fitting.

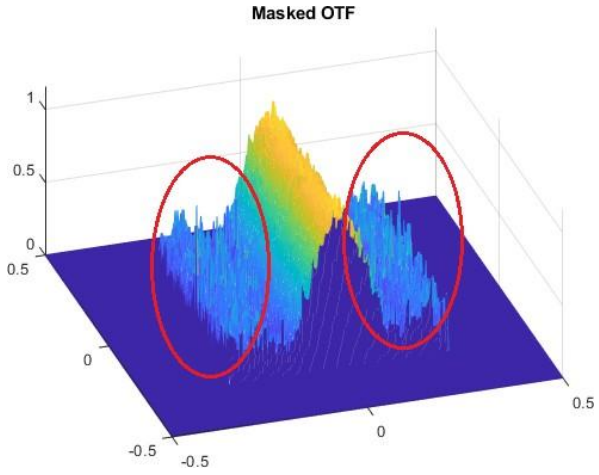

Figure 3. Example of masked motion OTF used for the sinc function fitting. The noisy components (in red circles) entering the cutting window make the estimation worse.

technique employs shifting of the reference image in frequency domain to obtain sub-pixel shifts in accurate way.

In this work, for convenience, the averaging technique is used even if motions with constant and uniform target speed during exposure time are considered. In this case, the obtained image is equivalent to the one obtained by applying the direct sinc function.

3. OPTIMIZATION OF MOTION BLUR ESTIMATION

3.1. Estimation technique

In this work, only referenced estimation has been considered, meaning that the availability of an image of the still target is always assumed, as it is usually the case in DIC measurements.

The estimation technique used in this work is based on the work presented in [1], where the motion is retrieved by the fitting of the experimental OTF computed from images with the sinc model previously presented. The experimental OTF $\mathcal{H}_{exp}$ can be computed as the ratio between the Fourier transform of the blurred and the reference image, referenced as $\mathcal{B}(k,l)$ and $\mathcal{R}(k,l)$, respectively:

$$\mathcal{H}_{\mathrm{exp}}(k,l) = \frac{\mathcal{B}(k,l)}{\mathcal{R}(k,l)}. \tag{4}$$

Once obtained, the experimental OTF can be represented in the 2D plane, obtaining an image made of parallel stripes inclined of ψ, which are the projection onto the horizontal plane of the lobes of the OTF (Figure 2).

Usually, the experimental OTF presents noisy points, especially for higher frequencies. Directly fitting the OTF would lead to poor estimation of the sinc parameters. For this reason, the motion parameters are estimated in a two-step procedure. At first, the experimental OTF is filtered by a median filter, and then binarized using a threshold to obtain a blob representing the main lobe of the sinc function: applying blob analysis, the inclination of the main lobe and so the motion direction is estimated with equation (3).

The sinc function fitting is hence performed with only the motion amount W as a free parameter. In Figure 3, an example of experimental OTF is shown; it is possible to see that the noise is less relevant for lower frequencies (the centre of the image corresponds to a frequency of 0). To reduce the effect of the noise in fitting results, only a restricted area of the whole domain is considered for the fitting. In [19], the width of the considered region, which will be called δ from now on, was fixed (90 spectral lines). In this work, the effect of different choices of δ is investigated, with the aim to obtain an optimal range for the δ definition.

The main idea is that, to maximise its effect, the δ parameter should be chosen according to the image size, since the size of the image determines the frequency resolution of the OTF and, hence, the number of spectral lines necessary to describe the sinc main lobe. In fact, the frequency domain of the OTF is in the interval $u \in \left[-\frac{f_s}{2}, \frac{f_s}{2}\right]$ and $\mathrm{v} \in \left[-\frac{f_s}{2}, \frac{f_s}{2}\right]$, being $f_s = 1\ \mathrm{px}^{-1}$ the sampling frequency, while the frequency resolution is $\Delta f_x = \frac{1}{D_x}$ and $\Delta f_y = \frac{1}{D_y}$ with D_x and D_y, the horizontal and vertical dimensions of the image, respectively. When D_x or D_y changes, the sampling frequency remains the same, but the frequency resolution changes, meaning that the extension of the subregion of the domain to be considered to isolate the main lobe of the OTF must change accordingly.

In this sense, it appears reasonable that an absolute optimal value for δ cannot be defined without considering the image size. For this reason, the parameter r defining the ratio between δ and image size is defined:

$$r = \frac{\delta_x}{D_x} = \frac{\delta_y}{D_y}, \tag{5}$$

introducing the possibility of having a rectangular cutting window in case of a rectangular image. In the following section, some tests on different images with the use of different values of r are presented, with the aim to define an optimal range for the parameter r.

3.2. Optimization of the r parameter

The estimation algorithm has been tested using images from a DIC challenge dataset [24]. Samples 3, 6, 9, and 14 (Figure 4) were selected since they have very different speckle types. Reduced versions of the original images in the dataset were used to limit the computation time for tests: square subregions of half side length were selected from the original images to obtain samples 3b, 6b, 9b, and 14b (where the letter 'b' identifies cropped images). Samples 3 and 9 were used also with the original size, to verify the hypothesis of the invariance of the r

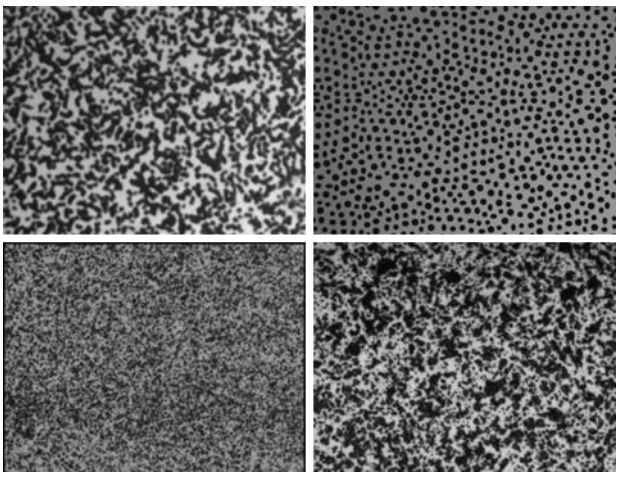

Figure 4. Sample images used for tests. Sample 3 (top-left), 6 (top-right), 9 (bottom-left), and 14 (bottom-right) from [13].

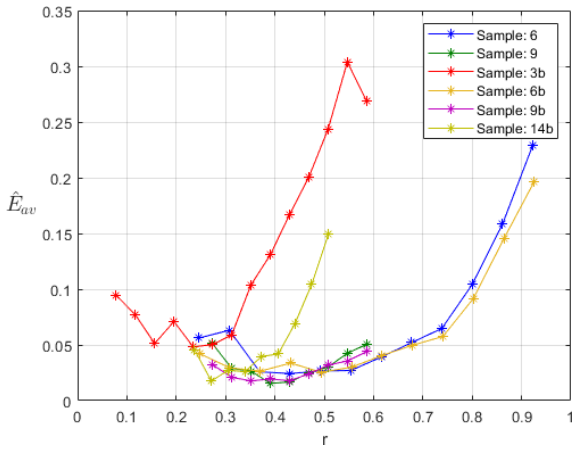

Figure 5. Mean blur amount estimation error, shown as a function of the image cutting ratio r for each tested sample type.

parameter from the image size. Images were numerically blurred, exploiting the averaging technique exposed in section 2.2. After the application of blur, white Gaussian noise with a standard deviation of 1 % of the image range has been applied, to simulate real acquisition noise. To obtain robust data describing general blur conditions, different kinds of motion blur have been simulated, varying both the direction and the amount of blur. For every image, four motion directions have been simulated (0°, 30°, 60°, 90°, with respect to the vertical axis). Seven values of motion amplitude, from 1.1 px to 7.7 px with steps of 1.1 px, have been considered.

Once the image datasets have been obtained, employing the estimation technique previously presented, the estimation of the blur has been repeated multiple times using different values of r, to verify the effect of the parameter on estimation output.

The goodness of the estimation has been evaluated as the relative difference between the real known blur amount W and the estimated one W_{est}:

$$\hat{E} = \frac{|W - W_{\text{est}}|}{W}. \tag{6}$$

To summarize results, for each image, the mean value of the estimation relative error is obtained as a function of the r parameter, as follows:

$$\hat{E}_{\text{av}} = \frac{1}{7}\frac{1}{4}\sum_{i=1}^{7}\sum_{j=1}^{4}\hat{E}(i,j)\,, \tag{7}$$

where i and j stand for the i-th and j-th values of motion amount (7 levels) and motion direction (4 directions), respectively.

Figure 5 shows the values of $\hat{E}_{\text{av}}$ as a function of r for each spackle type selected from DIC challenge. From this figure, different considerations can be made. First, we can note that the $\hat{E}_{\text{av}}$ vs r curve is not affected by the image size, as highlighted by the fact that the results for samples 6 and 6b are very similar, and the same stands for samples 9 and 9b. Moreover, the change in r affects the estimation results with a nearly parabolic trend. As expected, both too small and too large values of r, that is, of the cutting window size, lead to worse estimation. Too small values of r lead to the impossibility of having enough data for the fitting, while too large values lead to including noise disturbance at high frequency. Furthermore, for all the samples, the value of $\hat{E}_{\text{av}}$ reaches its minimum for values of r between 0.25 and 0.5, even if the optimal range is somehow influenced by speckle features, since different speckle types have different frequency contents. The sensitivity to changes of r is even influenced by the analysed speckle. For speckles characterized by high spatial frequency components and limited image noise (such as 6 and 6b), larger values of r allow to better handle the information content and therefore obtain lower error values. Summarizing all data, the range $r \in [0.25,0.50]$ appears to be optimal for all the considered samples.

4. MOTION BLUR COMPENSATION FRAMEWORK

Once motion blur parameters have been obtained, the blurred image can be manipulated to reconstruct the original still image. This operation can be performed by different techniques; traditionally, the most widely adopted are the Wiener filter [17], the Richardson–Lucy [21], and total variation techniques. Moreover, deep learning-based deblurring techniques have also been developed recently [22]. Traditional algorithms are widely used, in particular when high computation speed or real-time processing is needed. Since, in this work, computation speed is a relevant aspect, traditional deblurring methods were considered. According to recent literature, among traditional techniques, the Wiener filter is more suitable for most of the applications to minimize the effect of image noise [23], therefore it has been selected. Its mathematical expression is 0:

$$\mathcal{W}(k,l) = \frac{\mathcal{H}^*(k,l)}{\mathcal{H}(k,l) + \dfrac{|\mathcal{N}(k,l)|^2}{|\mathcal{R}(k,l)|^2}}, \tag{8}$$

where $\mathcal{H}^*$ is the complex conjugate of the motion OTF and $\frac{|\mathcal{N}|^2}{|\mathcal{R}|^2}$ is the noise to signal ratio (NSR), that is, the ratio between the autospectra of noise and reference noise-free image. Increasing noise levels amplify the instability of the inverse operation, requiring stronger regularization and consequently limiting the recovery of high-frequency details [25]. The correct application of Wiener filter hence requires, in addition to the motion OTF, the knowledge or the estimation of the NSR.

In this work, two different methods have been considered for the estimation of the NSR. The first method is based on a simple computation of the root mean square (RMS) of the reference image and an estimation of the noise amount performed with a method proposed by Liu et al. [26]. This noise

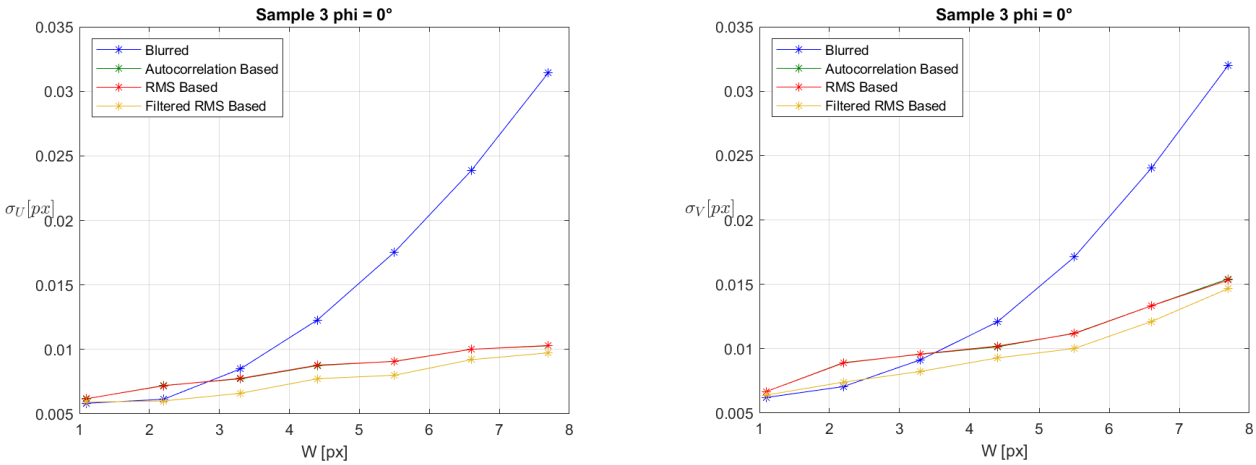

Figure 6. Example of DIC uncertainty referred to sample 3. The uncertainty (σ_u and σ_v for the horizontal and vertical directions, respectively) is computed for the blurred and the compensated images: values for different techniques for the NSR estimation are shown. The compensated images show an uncertainty reduction with respect to the blurred case; the reduction becomes more evident for higher values of blur.

estimation approach is based on principal component analysis applied on low rank patches of the image, that is, such regions with small variance. This approach has the advantage of working on a single image, even if its application is formally restricted to the case in which the noise is Gaussian. The NSR is hence computed as follows:

$$NSR_{\mathrm{RMS}} = \frac{\sigma_{\mathrm{N}}}{\sigma_{\mathrm{R}}}, \tag{9}$$

where σ_{R} is the RMS of the luminance profile of the reference image and σ_{N} is the noise level from the low patches analysis.

Some preliminary compensation tests performed with RMS estimation of the NSR show that usually a higher noise level is present in the compensated images, with respect to the reference ones. To mitigate this effect, the possibility to apply a Gaussian filter onto the compensated images has been considered.

The second estimation method considered is based on the analysis of the autocorrelation function of a single noisy image, as proposed by Thong et al. [27]. The NSR estimator is defined in the following way:

$$NSR_{\mathrm{autocorr}} = \frac{\alpha(0,0) - \alpha^{\mathrm{NF}}(0,0)}{\alpha^{\mathrm{NF}}(0,0) - \hat{p}^2}, \tag{10}$$

where $\alpha(0,0)$ and $\alpha^{\mathrm{NF}}(0,0)$ are the maximum values of the autocorrelations of the noisy image and the noise-free version of the image, respectively, and $\hat{p}$ is the mean value of the noisy image. Since, in this work, a noise-free version of the image is not considered to be available, the value of $\alpha^{\mathrm{NF}}(0,0)$ is not actually known. However, it is possible to give an estimation of $\alpha^{\mathrm{NF}}(0,0)$ using the properties of the noise autocorrelation. In particular, since the autocorrelation of the noise is a Dirac delta, and since this peak will be added to the peak of the noise-free image autocorrelation, with some approximation it is possible to assume that $\alpha^{\mathrm{NF}}(0,0)$ is a value similar to those assumed by $\alpha(x,y)$ in the neighborhood of the peak. For this reason, an approximation for $\alpha^{\mathrm{NF}}(0,0)$ can be:

$$\alpha^{\mathrm{NF}}(0,0) \approx \frac{\alpha(1,0) + \alpha(0,1)}{2}. \tag{11}$$

5. EFFECT OF MOTION BLUR COMPENSATION ON DIC RESULTS

The proposed optimized estimation and compensation procedure has been tested considering the effect of the motion removal on DIC analysis results. As already mentioned, the uncertainty of the displacement results is proportional to the amount of blur, meaning that, after the compensation, the uncertainty is expected to be reduced.

The tests were carried out considering the same set of images as used in section 3.2, analysing both the blurred and the compensated images with the commercial DIC software Vic-2D. Since in DIC measurements the image is divided into subsets and for each of these a value for the horizontal and vertical displacement is computed, if the actual motion of the target is rigid (i.e., displacements are uniform), the standard deviation of the obtained displacement can be directly taken as an uncertainty measure.

In Figure 6 shows the results in terms of uncertainty, considering the sample 3 speckle as an example. As expected, it is possible to see the parabolic increase of uncertainty with the increase of the motion blur amount, while the compensated images show an uncertainty reduction that becomes more evident for higher values of blur.

To analyse the effect of blur compensation on DIC uncertainty, the ratio between the uncertainty of the blurred image σ_{blur} and the uncertainty of the compensated image σ_{comp} is considered:

$$\hat{r}_\sigma = \frac{\sigma_{\mathrm{blur}}}{\sigma_{\mathrm{comp}}}. \tag{12}$$

The ratio $\hat{r}_\sigma$ has a straightforward meaning, being higher than 1 when the compensation leads to a reduction of uncertainty, and so to an improvement of DIC quality.

Figure 7 shows the results of the DIC test in terms of $\hat{r}_\sigma$ for all the considered speckle images. As already seen in Figure 6, also here, it is possible to observe that the effect of uncertainty reduction is proportional to the motion blur amount. When the motion blur is large, the improvement given by the compensation procedure is clear, then, for smaller values of W, the effect decreases, until, under a certain value of blur, the compensation appears to have negative impact on uncertainty.

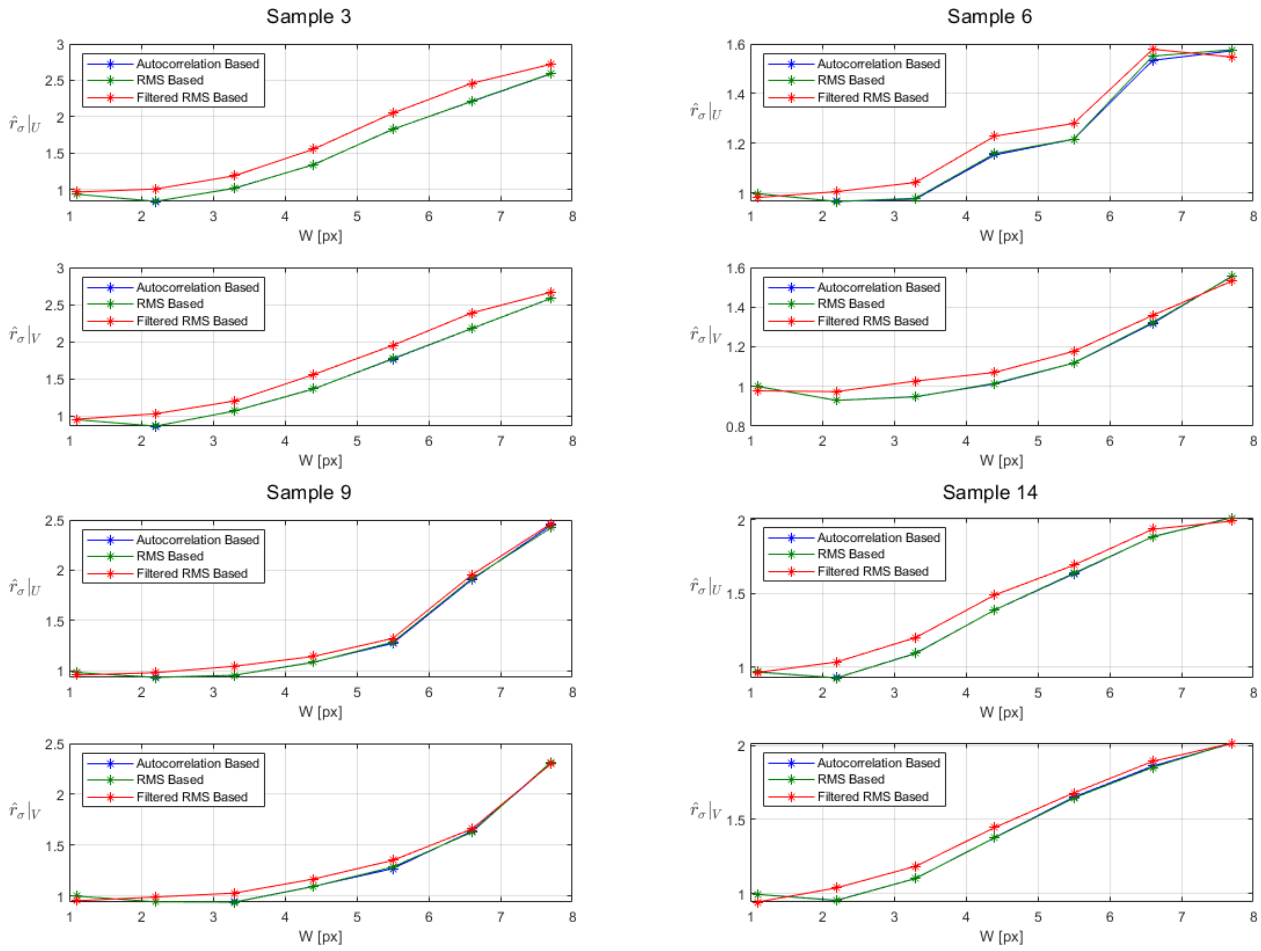

Figure 7. Results of tests on all samples in terms of the ratio between the uncertainty of the blurred images analyses and the compensate images analyses.

This behaviour is reasonable, since a small value of blur leads to a slight increase in the uncertainty of DIC: if this is case, the noise and possible artefacts introduced by the compensation procedure could create disturbances that have an effect worse than that of blur. This observation, in general, suggests that, for a small amount of blur, in the order of 1–2 px, the compensation could not have any benefit in terms of DIC results.

Figure 6 and Figure 7 show even the comparison between compensations carried out with different estimations of the NSR. RMS and autocorrelation methods appear to be equivalent when the effect on DIC is evaluated. The Gaussian filtering applied after the compensation with RMS methods demonstrate better performances, resulting in the strongest reduction of DIC uncertainty in all the considered cases.

6. CONCLUSIONS

In the present work, the effect on DIC analysis of motion blur, generated by the movement of the target or the camera during exposure time, is considered. Motion blur estimation technique based on motion OTF has been applied and optimized. Images with different kinds of speckle and several amounts of motion have been tested, to find optimal values for the estimation parameters. Then, compensation of motion blur based on the application of Wiener filter has been performed, considering different strategies for the image noise estimation. The performance of the proposed estimation and compensation procedure has been evaluated in terms of uncertainty of displacements computed with DIC, comparing the values obtained for blurred and compensated images. Results show that, in general, the optimized procedure has a positive effect on DIC performances, being able to reduce the effect of motion blur on uncertainty. This improvement is visible starting from values of motion blur of about 1–2 px, while for smaller blurs, the compensation does not appear that useful, since the image degradation due to blur slightly affects the uncertainty of DIC. The proposed technique is based on the hypothesis of constant motion blur in the image area. However, the same approach can be applied to subsets of the image, to improve the results in case of non-constant motion blur in the field of view: this is a further and straightforward generalization of the proposed technique.

REFERENCES

[1] B. Pan, Digital image correlation for surface deformation measurement: historical developments, recent advances and future goals, Measurement Science and Technology 29 (2018) 8, p. 082001.
DOI: 10.1088/1361-6501/aac55b

[2] H. Schreier, J. Orteu, M. A. Sutton. Image Correlation for Shape, Motion and Deformation Measurements, Springer, Boston (MA), 2009.
DOI: 10.1007/978-0-387-78747-3

[3] Y. L. Dong, B. Pan, A review of speckle pattern fabrication and assessment for Digital Image Correlation, Experimental Mechanics, 57 (2017), pp. 1161-1181.
DOI: 10.1007/s11340-017-0283-1

[4] J. Baqersad, P. Poozesh, C. Niezrecki, P. Avitabile, Photogrammetry and optical methods in structural dynamics - A review, Mech. Syst. Signal Process 86 (2016), pp. 17-34. DOI: 10.1016/j.ymssp.2016.02.011
[5] C. Warren, C. Niezrecki, P. Avitabile, P. Pingle, Comparison of FRF measurements and mode shapes determined using optically image based, laser, and accelerometer measurements, Mech. Syst. Signal Process. 25 (2011) 6, pp. 2191-2202. DOI: 10.1016/j.ymssp.2011.01.018
[6] W. Wang, J. E. Mottershead, A. Ihle, T. Siebert, H. R. Schubach, Finite element model updating from full-field vibration measurement using digital image correlation, J. Sound Vibrat. 330 (2011) 8, pp. 1599-1620. DOI: 10.1016/j.jsv.2010.10.036
[7] P. Poozesh, J. Baqersad, C. Niezrecki, P. Avitabile, A multi-camera stereo DIC system for extracting operating mode shapes of large scale structures, Proc. Annu. Conf. Experim. Appl. Mech. 3, River Publishers, 2016, pp. 225-238. DOI: 10.1007/978-3-319-22446-6_29
[8] M. Kalaitzakis, S. R. Kattil, N. Vitzilaios, D. Rizos, M. Sutton, Dynamic Structural Health Monitoring using a DIC-enabled drone, Proc. of the Int. Conf. on Unmanned Aircraft Systems (ICUAS), Atlanta, GA, USA, 11-14 June 2019, pp. 321-327. DOI: 10.1109/ICUAS.2019.8798270
[9] D. Reagan, A. Sabato, C. Niezrecki, Unmanned aerial vehicle acquisition of three-dimensional digital image correlation measurements for structural health monitoring of bridges, Proc. of SPIE - The International Society for Optical Engineering 10169, 2017, art. no. 1016909. DOI: 10.1117/12.2259985
[10] R. Balcaen, A. Lavatelli, C. Jiménez-Peña, E. Zappa, D. Debruyne, Impact of motion blur on stereo-digital image correlation with the focus on a drone-carried stereo rig, Strain 55 (2019) 1, 12300. DOI: 10.1111/str.12300
[11] J. Gu, L. Gang, L. Mengzhu, Damage Detection for Rotating Blades Using Digital Image Correlation with an AC-SURF Matching Algorithm, Sensors 22 (2022) 21, art. no. 8110. DOI: 10.3390/s22218110
[12] L. Wang, S. Bi, X. Lu, Y. Gu, C. Zhai, Deformation measurement of high-speed rotating drone blades based on digital image correlation combined with ring projection transform and orientation codes, Measurement 148 (2019), art. no. 106899. DOI: 10.1016/j.measurement.2019.106899
[13] A. Lavatelli, E. Zappa, Modeling uncertainty for a vision system applied to vibration measurements, IEEE Transactions on Instrumentation and Measurement 65 (2016) 8, pp. 1818-1826. DOI: 10.1109/TIM.2016.2541359
[14] A. Lavatelli, E. Zappa, A displacement uncertainty model for 2-D DIC measurement under motion blur conditions, IEEE Transactions on Instrumentation and Measurement 66 (2017) 3, pp. 451-459. DOI: 10.1109/ TIM.2016.2644898
[15] T. Chan, C.-K. Wong, Total variation blind deconvolution, IEEE Transactions on Image Processing 7 (1998) 3, pp. 370-375. DOI: 10.1109/83.661187
[16] S. Turrisi, E. Zappa, A. Lavatelli, Image deconvolution techniques for motion blur compensation in DIC measurements, Proc. of the 2018 I2MTC IEEE Instrumentation and Measurement Technology Conf., Houston, TX, USA, 14-17 May 2018, pp. 1-6. DOI: 10.1109/I2MTC.2018.8409567
[17] N. Wiener, Extrapolation, Interpolation and Smoothing of Stationary Time Series, 1st MIT paperback edn, Cambridge, MIT Press, 1964
[18] M. Potmesil, I. Chakravarty, Modeling motion blur in computer-generated images, Proc. of the 10th Annual Conf. on Computer Graphics and Interactive Techniques, Detroit, MI, USA, 25 - 29 July 1983, pp. 389-399. DOI: 10.1145/800059.801169
[19] A. Lavatelli, S. Turrisi, E. Zappa, A motion blur compensation algorithm for 2D DIC measurements of deformable bodies, Measurement Science and Technology 30 (2019) 2, 025401. DOI: 10.1088/1361-6501/aaf31a
[20] E. Zappa, P. Mazzoleni, A. Matinmanesh, Uncertainty assessment of digital image correlation method in dynamic applications, Optics and Lasers in Engineering 56 (2014), pp. 140-151. DOI: 10.1016/j.optlaseng.2013.12.016
[21] M. Thakur, S. Datar, Image Restoration Based On Deconvolution by Richardson Lucy Algorithm, International Journal of Engineering Trends and Technology (IJETT) 14 (2014) 2, pp. 161-165. DOI: 10.14445/22315381/IJETT-V14P232
[22] C. Jiang, L. Hu, G. Jia, The Application of Deep Learning in Image Deblurring. Proc. of the 2024 4th Int. Conf. on Artificial Intelligence, Big Data and Algorithms (CAIBDA '24), New York, USA, pp. 1075-1079. DOI: 10.1145/3690407.3690586
[23] V. Vasudev, M. V. Rajesh, A Comparative Study of Wiener, Richardson-Lucy, and Total Variation Techniques for Astronomical Images, Proc. of the 2024 IEEE Int. Conf. on Signal Processing, Informatics, Communication and Energy Systems (SPICES), Kottayam, India, 20-22 September 2024, pp. 1-4. DOI: 10.1109/SPICES62143.2024.10779775
[24] P. L. Reu, E. Toussaint, E. Jones, H. A. Bruck, M. Iadicola, R. Balcaen, D. Z. Turner, T. Siebert, (+ 2 more authors), DIC challenge: developing images and guidelines for evaluating accuracy and resolution of 2D analyses, Experimental Mechanics 58 (2018), pp. 1067-1099. DOI: 10.1007/s11340-017-0349-0
[25] R. Fergus, B. Singh, A. Hertzmann, S.T. Roweis, W.T. Freeman, Removing Camera Shake from a Single Photograph, ACM Transactions on Graphics (SIGGRAPH) 25 (2006) 3, pp. 787-794. DOI: 10.1145/1141911.1141956
[26] X. Liu, M. Tanaka, M. Okutomi, Single-image noise level estimation for blind denoising, IEEE Transactions on Image Processing 22 (2013) 12, pp. 5226-5237. DOI: 10.1109/TIP.2013.2283400
[27] J. T. L. Thong, K. S. Sim, J. C. H. Phang, Single-image signal-to-noise ratio estimation, Scanning 23 (2006) DOI: 10.1002/sca.4950230506